Project Summary

Effects of Microstructural Anisotropy on the Mechanical Response of Aluminium Alloy AA 7010 – T7651

AL Cranston[1]

University of New South Wales at the Australian Defence Force Academy

The effect of microstructural anisotropy on the mechanical response of a heavily rolled 7010 – T7651 has been investigated. A comprehensive set of quasi-static and dynamic experiments were conducted on specimens loaded along the Rolling (RD) and Through Thickness (TT) directions. Results suggest that specimens tested along their TT exhibit higher Elastic limit and Moduli; whereas specimens tested along their RD will exhibit higher ductility and fracture stress. These observations held true for both the quasi-static and shock-loaded specimens. Optical and EBSD characterisation was performed on a number of the deformed specimens to investigate this behavior. For the case of shock-loaded specimens, it was found that void nucleation was dependent on grain orientation with respect to the applied load, whereas angle misorientation and Taylor factor did not contribute significantly.

Contents

Nomenclature

AA = Aluminum Alloy
Al = Aluminum
ASTM = American Society for Testing and Materials
Cu = Copper
EBSD = Electron backscatter diffraction

[1] SBLT, School of Engineering & Information Technology. ZEIT4500

HEL = Huginiot elastic limit
HET-V = Heterodyne Velocimeter
Mg = Magnesium
RD = Rolled direction / Transverse direction
SD = Standard deviation
TT = Through Thickness/Short Transvers direction
TWIP = Twinning-induced plasticity
Zn = Zinc
Zr = Zirconium

I. Introduction

A study into the microstructural anisotropy of the common Aluminium alloy 7010 T7651 was conducted to provide a better understanding of microstructural explanations for changes in strength properties due to anisotropic microstructure when rolled. The aluminium tested is a high strength aluminium alloy designed for applications where strength to weight ratios are important, and has the potential to be used for armour applications. It has a tensile stress of 472MP, and can be strengthened and hardened by cold working or heat treatment. The standard alloying elements for 7010 alloy is detailed in Table I [1].

Table I. Specification of alloy elements of 7010 and 7075 AA by wt.%

Zn	Mg	Cu	Zr	Fe	Si	Ti
5.7-6.7	2.1-2.6	1.5-2.0	.10-.16	0.15 max	.12 max	.006 max

Source [2] explains the treatment T7651 as being solution heat treated, and stress relieved then artificially overaged in order to achieve a good exfoliation corrosion resistance. Solution heat treatment involves the deliberate alteration of the properties through dissolving of the alloying elements at temperatures 460–560 °C, altering its structure to make it more homogenous. Age hardening is also achieved through long-term exposure to room temperature or a slightly elevated temperature. Since the alloying elements have a decreased solubility with the decrease in temperature, this will lead to those elements precipitating out of solution with the formation of fine, uniformly distributed particles that will block the slip planes and obstruct the movement of dislocations. There is a corresponding increase in strength [3].

Other Al alloys have also been studied to ascertain the mechanical strength properties and spall behavior due to grain size [4-5] using similar experimental techniques. In [5] both pure and AA 1050 were cold rolled, and then annealed and heat treated to specific conditions in order to gain specific grain sizes before testing. The post-mortem characterisation concluded that at sufficient stresses spall response in pure Al does in fact increase with grain size increases, however for the alloyed 1050 there was no significant difference. In an experiment conducted by Boteler et. al [6], the dynamic response of two differing 5083AA tempers, being Al5083-H131 (H131) and Al5083-H32 (H32) were discussed. In the report, it was noted that Aluminium Alloy Al5083 has been a preferred material for armour for many military vehicles. Their report explains how the transition between elastic to plastic response occurs at the material HEL. The average HEL parameters that they found are detailed in Table II. in this instance, the strain-hardened temper H131 displayed the most elastic-plastic response.

Table II. Average HEL Parameters

Temper	HEL (GPa)
H32	0.40 ± 0.03 GPa,
H131	0.573 ± 0.04 GPa,

Previous experiments conducted by Paul Hazel et al [7] look into the properties of AA 7010-T7651 through plate impact and quasi-static tensile tests on specimens in the RD and TT direction, in order to examine the shock response to shock wave-loading through the Huginiot Elastic Limit (HEL) and the dynamic tensile strength characteristics. It was found that the RD direction displayed higher yield strength, ultimate tensile strength, and almost double the amount of elongation that the samples from the short-transverse directions. The dynamic tensile behavior was also evaluated through changes to impact stress in both directions. The results show the RD direction to have approximately 30% increased spall strength than that of the TT direction. These results were relatively high in comparison to other high strength aluminum alloys [6], and therefore it was concluded in that paper that it would make a good choice for amour applications. However, this particular

experiment does not look into the microstructural reasons for this behavior. Therefore, a number of specimens from this experiment were used for microstructural characterisation.

II. Experimental Methods

In order to accurately examine how the microstructure is affected through various impact methods, EBSD images of both the rolled (RD) and through-the-thickness (TT) planes of an as-annealed specimen of Aluminium alloy 7010 T7651 were taken as a control. Images shown in Fig 1 show that along the rolled direction, the material is textured towards the 111 planes.

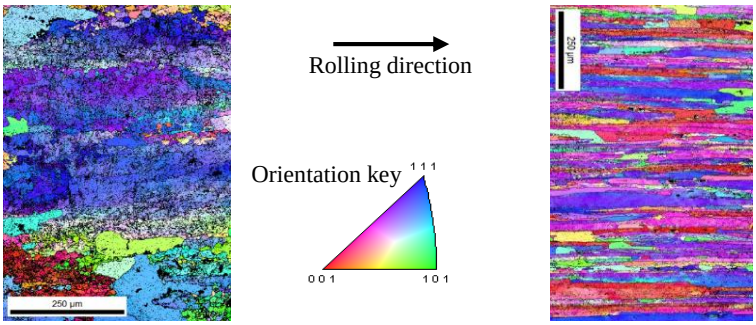

Figure 1. Images of as annealed AA 7010 T7651 in the: a) rolled direction and b) transverse direction

A. Quasi-Static Testing

Compression experiments were designed and executed in accordance with ASTM E9-09 [8]. ASTM E9-09 is a standard which details the test methods for compression testing of metals at room temperature. Small cylinders 7mm in diameter and length were machined with their compression axis oriented along either the rolling direction (RD), transverse direction (TD) or through-thickness direction (TT). Figure 2 shows how the directions correlate to the original as annealed plate.

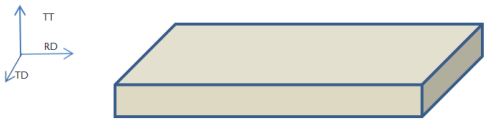

Figure 2. orientation of directions during testing

The tensile experiments were also conducted following the respective standard utilizing "dogbone" specimens [8-9]. Tests were carried out using a Shimadzu machine at a strain rate of ~10^{-3}/s. The force applied and displacement was recorded for both sets of trials. From this data, and the geometric information of the specimens, stress strain data could be ascertained and used for analysis of mechanical response.

B. High strain- rate testing

For the dynamically loaded experiments described in [7], four specimens in both the RD and TT directions were impacted at 200, 500, 700, and 900m/s using a 50-mm single stage gun with 1050 Al flyers (results of only the first two impact velocities are provided in this article). Plate impact testing is commonly used in investigating dynamic damage evolution and failure mechanisms of metals, composites, and many other materials [10-12]. The plate impact experiments consist of a thin plate or flyer plate that is launched against a target of the same or similar material properties. Upon impact an initial elastic shock compressive state is generated, then upon decompression is followed by a plastic release waves that travels from the free surface towards the target, causing a tensile stress in the interior specimen area at strain-rates on the order of 10^3-10^5 /s [13]. An image of a post-impacted target plate is shown in Fig 3.

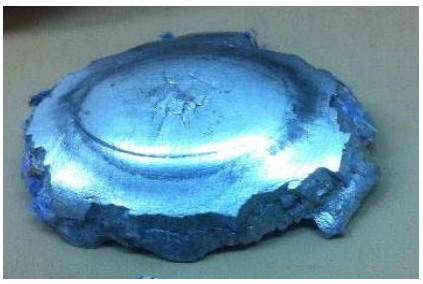

Figure 3. TT target sample impacted at 718m/s

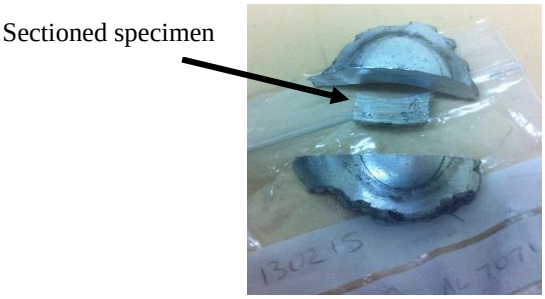

Figure 4. Sectioned specimen ready for mounting and characterization

Transmission of the shock wave was evaluated using a Heterodyne Velocimeter (Het-v). This method is useful for the measurement of dynamic strength, in specific the Hugoniot elastic limit (HEL) and the spall strength [4, 7, 14-15]. The experimentally obtained spall strength of a material is often determined through its measured velocity pullback [16]. The velocity pullback is defined by the FSV difference experienced by the material. The spall strength (σ_{sp}) was estimated by utilizing [17]:

$$\sigma_{sp} = \frac{1}{2}\rho_0 c_b(\Delta FSV + \delta_{corr}) \quad (1)$$

In general the TT direction is generally the less ductile. Therefore, it was expected that the TT specimens fail in a less ductile manner than the RD specimens when impacted [18]. The HELs in each test were also calculated from the free-surface velocity using the following equation [19]:

$$\sigma_{HEL} = \frac{1}{2}\rho_0 c_l u_{fs} \quad (2)$$

Note: *ufs* is the free-surface velocity taken from the point at which the elastic wave transitions to the plastic wave. The HEL is a measure of dynamic yield strength under uniaxial strain loading [4], and prescribes the locus of all possible states attainable by single stage shock compression from an initial state [11]. HEL can be related back to the material Yield strength through the following equation [21]:

$$\sigma_Y = \left[\frac{(1-2v)}{1-v}\right]\sigma_{HEL} \quad (3)$$

Selected specimens were then sectioned with a low speed diamond blade to slice a small selection of each of the four experiments, as shown in Fig 4. Each specimen was then labelled with experiment number, direction of material cut (TT/ RD), and approximate FSV.

C. Characterisation

1. Optical

The tested materials were then set into an epoxy resin. The compressed samples were prepared by hand, using manual polish techniques from rough sandpaper, all the way through to vibro-polishing. The tested tensile and shock-loaded specimens were prepared using an automated Stuers polishing machine, previously unavailable for use with the compression samples. The machine improves the sample results as it automates and standardizes the sample prep process, as well as significantly reducing the amount of preparation time. All materials were then prepared for optical characterization by chemical etching using Keller's etch. This is a commonplace metallographic etchant for aluminum and its alloys when trying to reveal grain size [22]. The etching time typically takes around 10-20 seconds. A breakdown of the etchants composition is included in Table III. [23]

Table III. Keller's Etchant chemical breakdown

Product	Distilled water	Nitric acid	Hydrochloric acid	Hydrofluoric acid
Concentration	190ml	5 ml	3 ml	2 ml

Optical characterisation was performed using a Zeiss optical microscope equipped with an automated stage. This was performed to assist in determining the location of voids and grain boundary size and locations in the failed specimens. Then, the program *ImageJ* was used to assist in this analysis. ImageJ is a java based image processing software created to assist in optical analyses. Not only did it allow for manipulation of the image to

create a better visual of the damage or fracture surface, but the program can also calculate the overall and average area of all the damage, through the 'analyse particles' function.

2. Electron Back Scatter Diffraction

EBSD measurements were also performed on selected shock-loaded specimens [24]. During EBSD, The polished sample is placed in a SEM and inclined approximately 70° relative to normal incidence of the electron beam, which forms particular patterns on a fluorescent screen that is characteristic of the crystallographic structure and orientation of the sample, with sub-micron resolution [25].

Patterns created using the EBSD technique occur when the primary beam interacts with the material, subsequently the atoms scatter a fraction of low energy electrons that are subject to different path differences, causing constructive and destructive interference patterns. When used to form an image on the fluorescent screen the regions of enhanced electron intensity between the cones produce Kikuchi bands of the electron backscatter diffraction. [26] To ensure uniformity in the analysis, the same specimen reference frame was used for all EBSD images, i.e. RD aligned with the sample normal. From these images, a number of measurements were made using the processing program OIM to determine how, or if the grain boundary orientation affects the damage evolution.

A complementary type of analysis used was Taylor factor. These maps can assist in understanding deformation in materials [27-29], as it identifies hard and soft orientated grains. The Taylor factor relates the uniaxial yield stress and resolved shear stress. [30-31]. In [26] it is demonstrated that the Taylor factor can give an important guideline for determining the deformation mode of Twinning-induced plasticity (TWIP) steel. Because it is a function of grain orientation and applied stress, and its value indicates a specific plastic deformation mode under an applied stress.

III. Results

A. Quasi-static compression

The images displayed in Fig 5 show the stress-strain response curves of each of the three directions of loading. All had similar curves; however the rolled samples did yield at a slightly lower stress than the other two. Table IV also indicates that curve 1 and 3 have very similar responses, while the specimen compressed along the rolled direction showed reduced yield stress.

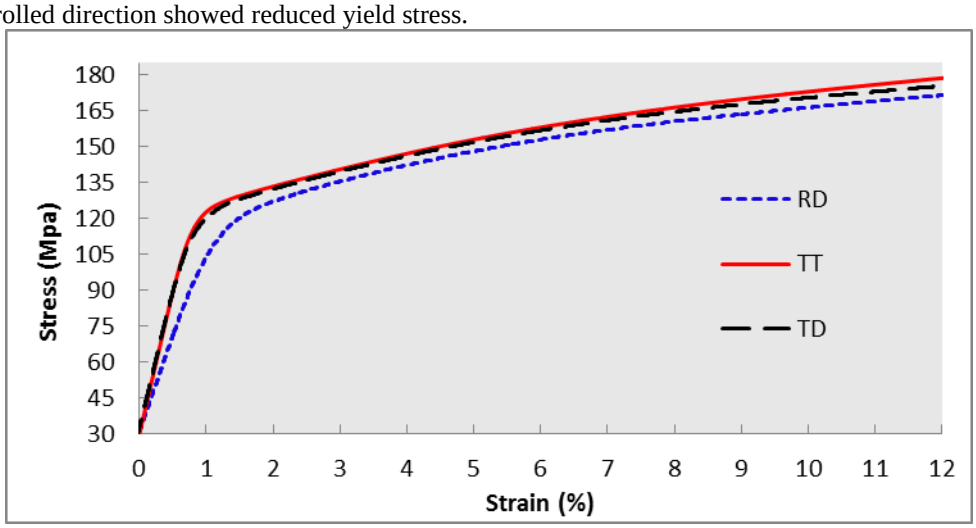

Figure 5. Stress strain diagram of compressed samples in TT and RD directions

Table IV. Yield stress analysis for compression tests on AA 7010 T7651

Direction	Yield stress (MPa)	Strain at yield (%)
RD	120 ± 2	1.22 ± 0.95
TT	125 ± 1.5	1.10 ± 0.02
TD	124 ± 4	1.15 ± 0.03

After compression tests were conducted, a sample of RD and TT specimens were chosen for optical analysis. The image in Fig 6a shows the grain boundaries are aligned parallel to the direction of loading in the RD

sample, whereas Fig 6b shows the TT sample has grain boundaries orientated perpendicular to the direction of loading. It was also noted that the grain boundaries in the RD specimen were slightly separated through the mid-section of loading. This behavior may be explained due to the fact that when the force is applied along the transverse direction, there is an increased grain boundary density, leading to an increase in resistance to dislocation impediment [32].

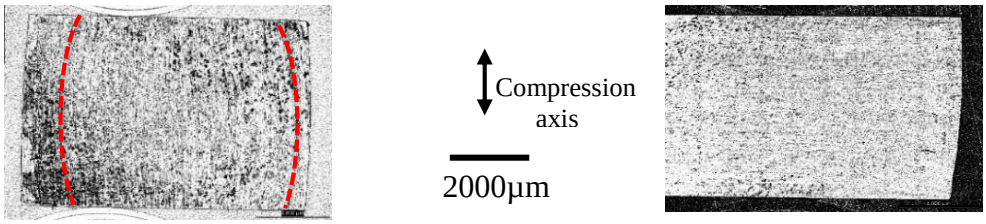

Figure 6. Optical micrographs of deformed specimens with compression axis along (a) RD and (b) TT directions. The superimposed lines show grain deformation.

B. Quasi-static tension

The stress strain curves in Fig 7 show that that the RD specimen deforms in a much more ductile way than the TT specimen. The data presented in Table V indicates all specimens experience the same yield stress. However, interestingly both The RD and TD specimens seem to fail with a more ductile behavior. Both reached a higher max stress, and then failed at a lower (engineering) stress. This is in contrast to the compression samples, where the rolled specimen alone exhibited different behavior to the other two samples.

From the accompanying images in Fig 8, it was observed that the RD specimens show a grain structure that is parallel to the applied force, where the TT specimens showed a perpendicular grain structure. It would be reasonable to conclude that because the grains of sample 2 are perpendicular to the applied stress, once voids began to appear they will easily nucleate across the grain boundaries, leading to a less ductile fracture at lower stresses. Where the other 2 samples also cracked along their grain boundaries, it was a lot harder to propagate across the width of the specimen as it had to find ways to cross those grains.

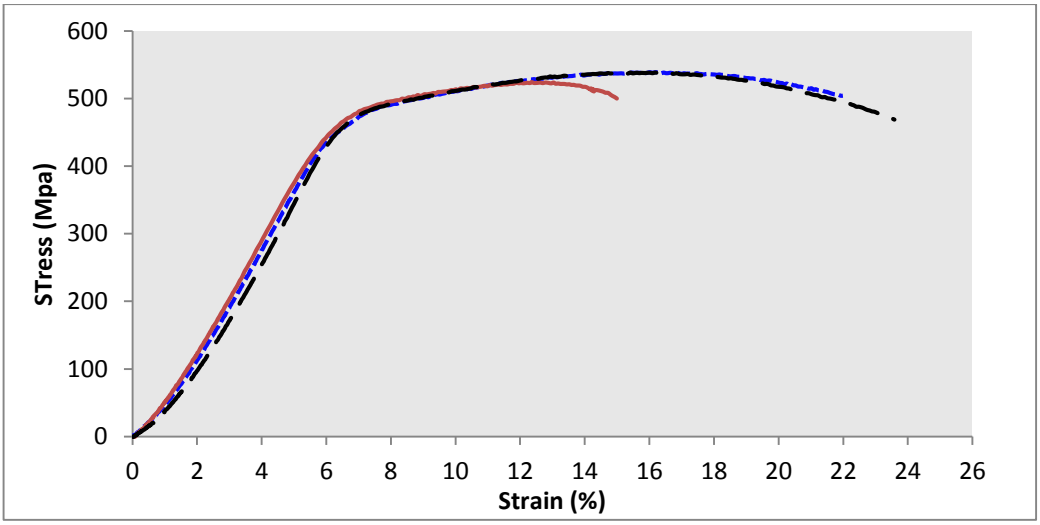

Figure 7. Stress strain diagram of compressed samples in TT and RD directions

Table V. Yield stress analysis for tensile tests on AA 7010 T7651

Direction	Yield stress (MPa)	Averages Stress at failure (MPa)	Strain at failure	Averages max stress (MPa)	Strain at max stress
RD	473 ±11.4	432 ±12.7	0.262 ±0.007	540 ±11.2	0.166 ± 0.009
TT	473 ±1.8	490 ±7.2	0.151 ±0.005	525 ± 3.8	0.125 ± 0.002
TD	475 ±1.4	456 ±5.7	0.242 ±0.004	540 ± 0.7	0.162 ± 0.009

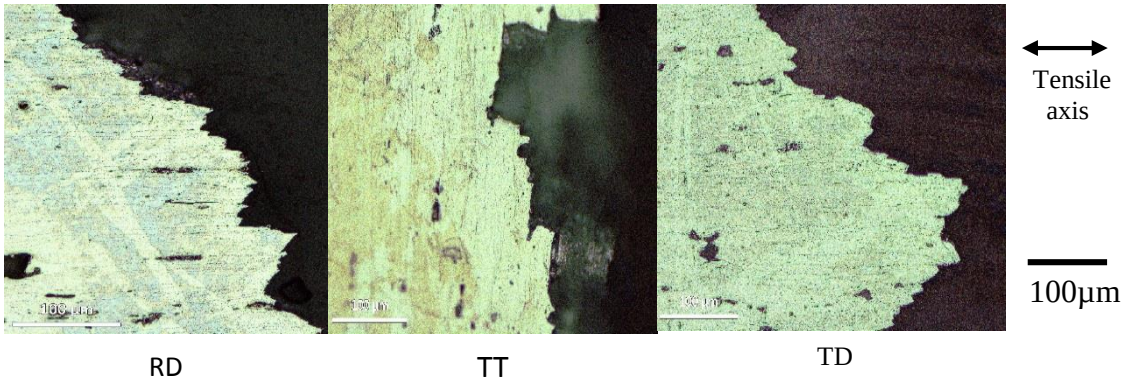

Figure 8. Optical images of tensile fracture surface profiles.

C. Shock-loading testing

The free surface velocity (FSVs) traces of experiments conducted at flyer velocities of ~190 and 490 m/s on RD and TT specimens are shown in Fig 9. At both impact velocities is observed that the change in FSV from the peak to the minima is higher in the RD oriented specimens. This change in FSV is generally associated to the spall strength of the material. A higher resistance for damage evolution is expected for the RD specimens, similar to the quasi-static tensile results. The results listed in Table VI illustrate the ΔFSV values from the previous plot, which were used to calculate spall strength using Eq. 1. With the exception of the RD-180m/s experiments which displayed no pullback signal, the spall strength in the RD direction was 34% greater than those tested in the TT direction

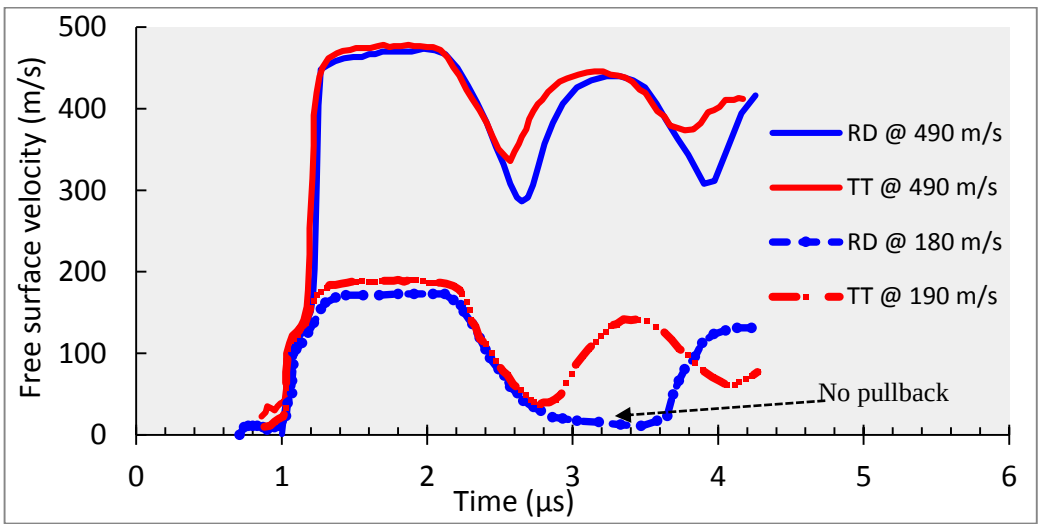

Figure 9. Free surface velocity traces for specimens impacted at ~190 and 490m/s

Table VI. Spall strength for shock-loading tests on AA 7010 T7651

Impact velocity (m/s)	ΔFSV RD (m/s)	Spall strength RD [GPa]	ΔFSV TT (m/s)	Spall strength TT [GPa]
180-190	No Spall (180-190)	No spall	141	1.21
490	186	1.62	150	1.22

Optical microscopy images shown in Fig 10 illustrate the damage experienced by the same specimens as in Fig 9. In Fig 10a, it can be seen that the RD specimen impacted at 180m/s did not actually experience spall damage, as data in Fig 9 suggests by the lack of pull back wave. The TT specimen impacted at a similar speed of 190m/s did experience a crack spanning through the middle of the specimen. The image in Fig 10c shows the resulting damage. Comparing the two specimens impacted at around 500m/s in Fig 10b and 10d, it is observed that the RD specimen exhibits limited evidence of damage with voids oriented along the grain boundaries, parallel to the shock direction. Whereas, the TT specimen shows a considerably higher amount of damage, in this case the voids coalesce perpendicular to the direction of loading.

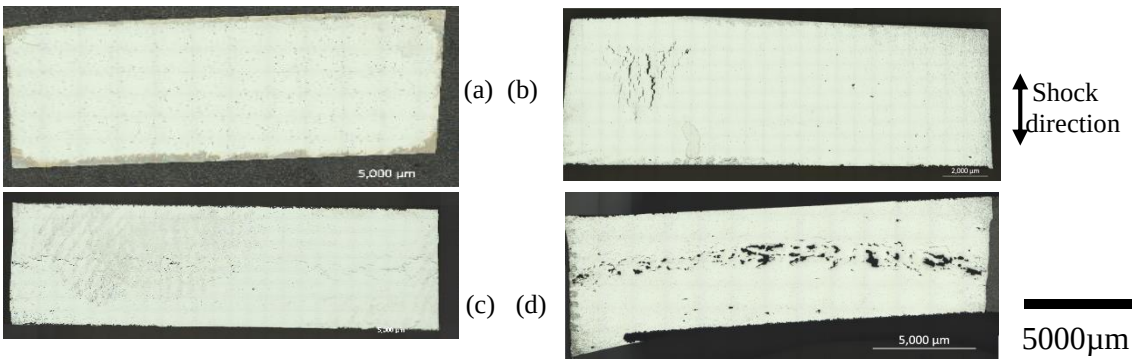

Figure 10. Optical images of spalled samples of (a) RD impacted at 180m/s (b) RD at 490m/s (c) TT at 190m/s (d) TT at 490m/s

The calculated HEL values in each direction are also presented in Table VII. HEL was described in Eq. 2 as the stress where the elastic wave transitions to a plastic wave, and is closely related to yield strength (Eq 3). While the RD direction has shown to exhibit higher spall strength, the transverse direction has displayed a higher HEL. This is interesting because the HEL is concerned with the initial compressive wave, and this response was also experienced in the yield stresses on the quasi-static compression tests. As with the quasi-static compression test, this is likely to be due to the higher rate of dislocation impediment when force is loaded along the TT.

Table VII. Experimental spall strength and HEL measurements from plate impact tests

Average HEL Data (GPa)	
RD	TT
0.89 ±0.02	0.95 ±0.02

EBSD measurements were performed on spalled regions in both the RD and TT directions. The results are shown in Fig 11. In both the RD and TT specimens, cracks run along the grain boundaries. Furthermore, these images allowed assessment of whether crystallographic orientation between grains affected the locations where cracks nucleated. This was done by measuring the misorentation between grains that have spall damage, as opposed to grains that did not. For both the RD and TT specimens the misorientation angles in spalled GBs was in the 10-60º range; similar values were obtained for the misorientation angles on GBs that did not spall.

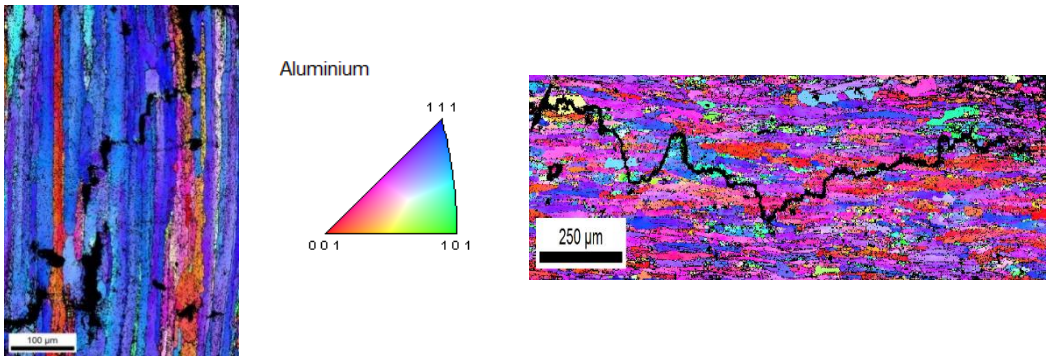

Figure 11. (a) RD impacted sample (b) TT impacted sample

However, upon investigation both samples selected from regions where damage had occurred and unaffected areas had the same range of misorientation between grains (between 8-60 degrees). This leads to the conclusion that misorientaiton between grains cannot be used to predict damage growth. Taylor factor maps of the specimens were also produced to determine if there was evidence that damage propagates preferentially along grain boundaries with different hardness values, and at what level that might begin to effect damage evolution. Fig 12 is a representative Taylor map of spalled sections in the rolled direction. While there are some cases where the damage nucleated is between grains of high difference, there are just as many areas of damage between grains of similar strength. Again, this indicates that prediction of damage location within the AA cannot be determined through examining the Taylor factor, or hardness variations between grains.

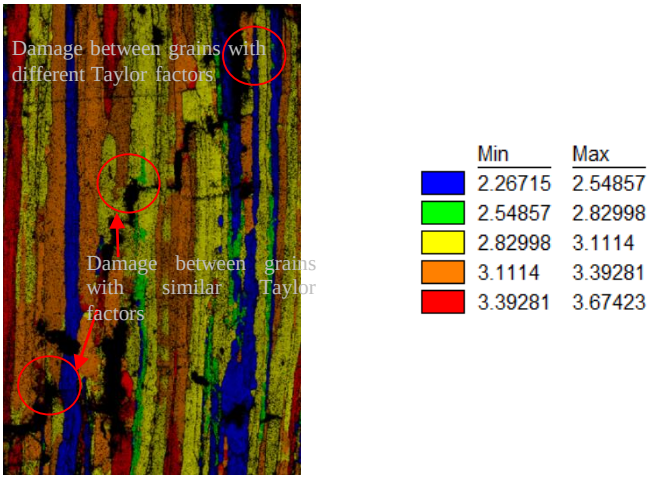

Figure 12 – Taylor Map of spalled sections of a rolled specimen

IV. Conclusions

This research project aimed to identify microstructural effects on the directional strength properties of AA 7010 T7651. Under quasi-static compressive loads it was seen that the TT direction showed slightly increased yield strength when compared to the RD samples. This was attributed to an increased grain boundary density, leading to an increase in resistance to dislocation impediment. During the initial shock compressive state in the plate impact tests, this behavior was also seen in the increased HEL values for specimens loaded along the TT direction. However, in the quasi-static tensile and plate impact samples it was shown that there was higher spall strength displayed when loaded along the RD plane. EBSD measurements, angle misorientation and Taylor factor, suggest that these properties play little significance in where or how the material failed. Overall, our results indicate that grain boundary orientation with respect to the applied load is the main factor affecting tensile, quasi-static and dynamic, material failure. Specimens can withstand a higher level of plastic deformation in the RD, whereas the TT samples tend to fail more readily along the grain boundaries.

V. Recommendations

The testing to date has only looked at quasi-static and plate impact tests. Dynamic tests such as Hopkinson bar tests and drop tower tests on the same materials would round out the research done. Since the research was conducted on a collection of separate tests, it was impossible to trace back the exact processing the material experienced, or how was the plate cut from the rolled material. In order to respond to the questions raised during testing about if or how this may affect results, more tests would have to be conducted, where all plates were cut and tested from the same machined material. Preferably these tests would span across the entire spectrum of available quasi-static, dynamic, and impact testing methods.

In order to expand on the work already done to date, in-depth research into crystallographic orientation effects should also be conducted. This should include looking at other properties such as elastic moduli, Schmid factor, *etc*, along the spall plane where the material did spall, compared to sections along the spall plane where they did not to see if there is any correlation.

VI. Acknowledgements

I would like to start by thanking my thesis supervisor, JP Escobedo for all his assistance, guidance and advice throughout the year. I would also like to acknowledge the contributions of David Sharp for his assistance in conducting the quasi-static tests and sample preparation throughout the year. Stuart Gay is also thanked for assisting with the design and manufacturing of specimens used for testing. Finally, Paul Hazell is also thanked for providing tensile and spall samples for the characterisation process that complemented this project.

VII. References

[1] J.S. Robinson, D.A. Tanner, C.E. Truman, A.M. Paradowska, R.C. Wimpory, (2012) '*The influence of quench sensitivity on residual stresses in the aluminum alloys 7010 and 7075,* **Materials characterization,** 6 5, pp. 7 3 – 8 5

[2] Alumeco. (2014). *'Alumeco - Temper descriptions'*, (online) Available: http://www.alumeco.com/Technical_information/Temper_description.aspx [Accessed 14 March 2014]

[3] AluminiumIndustry.org, (2014),*'Aluminum Strengthening Mechanisms'*, Available: http://www.aluminiumindustry.org/en/aluminum-strengthening-mechanisms.html[Accessed 14 March 2014]

[4] P. B. Trivedi, J. R. Asay, Y. M. Gupta, and D. P. Field,(2007), '*Influence of grain size on the tensile response of aluminum under plate-impact loading',* ***Journal of Applied Physics*** 102, 083513

[5] Adam J. Schwartz, James U. Cazamias, Peter S. Fiske, and Roger W. Minich, (2002). '*Grain Size and Pressure Effects on Spall Strength in Copper',* ***American Institute of Physics*** Conf. Proc. 620, 491

[6] J. Boteler, D. Dandekar, (2006), '*Dynamic response of two strain-hardened aluminum alloys'* **Journal of Applied Physics** 100, 054902

[7] P.J. Hazell, G.J. Appleby-Thomas, D.C. Wood, and J.D. Painter, '*The shock and spall response of AA 7010-T7651'*

[8] ASTM. (2009). '*Standard Test Methods of Compression Testing of Metallic Materials at Room Temperature.'* ***ASTM E9-09***

[9] Instron, '*Tension testing of mettalic materials (ASTM E8)',* (online) Available: http://www.instron.com.au/wa/solutions/astm_e8_tension_testing_metallic_materials.a [Accessed 01 june 2014]

[10] J.P. Escobedo, E.K. Cerreta, and D. Dennis-Koller, (2013), *'Effect of Crystalline Structure on Intergranular Failure during Shock Loading',* ***JOM*** Vol 66 2014

[11] A. Gfinicki, A. Vautrin, P. Soukatchoff, J. Franfois-Brazier, *'Plate Impact Testing Method for GRC Materials*', ***ELSEVIER Cement & Concrete Composites*** (1994) 241-251

[12] A. Enfedaque, D. Cendón, F. Gálvez, V. Sánchez-Gálvez *, (2011)'Failure and impact behavior of facade panels made of glass fiber reinforced cement(GRC)'**Engineering Failure Analysis 18,*** 1652-1663.

[13] D.R. Curran, L. Seaman, and D.A. Shockey**,** (1987), *'Dynamic Failure Of Solids',* **PHYSICS REPORTS** (Review Section of Physics Letters) 147, Nos. *5* & 6 253—388.

[14] R. Minich, J. Cazmais, M. Kumar, and A. Schwartz, (2004), *'Effect of Microstructural Length Scales on Spall Behavior of Copper',* **METALLURGICAL AND MATERIALS TRANSACTIONS A**. 2664—Vol 35A

[15] Escobedo, J. P, D. Dennis-Koller, E.K. Cerreta, B.M. Patterson, C.A. Bronkhorst, B.L. Hansen, D. Tonks, and R. A Lebensohn, (2011). *'Effects of grain size and boundary structure on the dynamic tensile response of copper'*, **Journal Of Applied Physics** 110, 033513

[16] X. Chen, J. R. Asay, A and S. K. Dwivedi, 2006, '*Spall behavior of aluminum with varying microstructures',* **Journal of Applied Physics**, Vol 99 023528

[17] S. V. Razorenov, G. I. Kanel, G. V. Garkushin, and O. N. Ignatova, (2012) '*Resistance to Dynamic Deformation and Fracture of Tantalum with Different Grain and Defect Structures'*, **Physics of the Solid State**, Vol. 54, No. 4, pp. 790–797.

[18] P. Hazel, (2014), '*Impact Dynamics' – week 3 Notes',* UNSW. Page 19

[19] J. Boteler, and D. Dandekar, (2006), '*Dynamic response of two strain-hardened aluminum alloys'* Journal of Applied Physics. **100** 054902

[20] T. Neal, (1977), '*Second Hugoniot Relationship for Solids',* **Journal of Physics and Chemistry of Solids.** Vol. 38. pp. 225-231.

[21] N. Bourne, J. Millett, M. Chen, J. McCauley, and D. Dandekar, (2007) *'On the Hugoniot elastic limit in polycrystalline alumina'* **Journal of Applied Physics** 102, 073514

[22] Etchant Store of ES Laboratory, LLC (2014) (online), Available:http://www.etchantstore.com/Kellers-Reagent-250-mL-161.htm [Accessed 07 Jun 2014]

[23] Pace Technologies, *(2014),* '*Metallographic Etchants – Aluminum',* Available:http://www.metallographic.com/Etchants/Aluminum%20etchants.htm [Accessed 07 Jun 2014]

[24] B. Adams, S. Wright, and K. Kunze, (1993)*, 'Orientation Imaging: the emergence of a new Microscopy'* **Metallurgical Transactions A,** Vol. 160(2), pp.229-240

[25] S. Swapp, (2014). '*Electron Backscatter Diffraction (EBSD).*' (online) Available: http://serc.carleton.edu/research_education/geochemsheets/ebsd.html [Accessed 01 May 2014]

[26] S. Sitzman, T. Maitland. (n.d.). *Electron Backscatter Diffraction (EBSD) technique and materials characterisation examples.*

[27] D. Dingly, (2012), Tutorial 3 – 'T*he importance of orientation measurement in polycrystalline materials'*, (online), Available:http://www.ebsd.org.uk/tutorial_3.html [Accessed 12 Sep 2014]

[28] X. Duan, D. Wang, K. Wang, and F. Han, (2013) '*Twinning behaviour of TWIP steel studies by Taylor Factor analysis'*.

[29] U. Kocks, H. Mecking, (2003), *Physics and Phenomenology of strain hardening: the FCC case*, **Progress in Materials Science** 48 171–273 2002 2

[30] R.E. Stoller, S.J. Zinkle, *(2000), 'Mechanical Behavior of Irradiated Materials on the Relationship between Uniaxial Yield Strength and Resolved Shear Stress in Polycrystalline Materials',* **Journal of Nuclear Materials** *283-287*

[31] H. Mecking, U.F. Kocks, and Ch. Hartig, (1996), '*Taylor Factors In Materials with many Deformation Modes',* **Scripta Materialia,** Vol. 35, No. 4, pp. 465-471

[32] W. Callister, Jr., (2007), *'Materials Science and Engineering'* (7th ed.), **McGraw-Hill**, p188-189